24th COBEM - 2017

24th ABCM International Congress of Mechanical Engineering
December 3-8, 2017, Curitiba, PR, Brazil

COBEM-2017-2304
DIGITAL RADIOGRAPHIC INSPECTION AND CHARACTERIZATION OF DEFECTS IN JOINED ALUMINUM ALLOY AA5083 FOR SHIPBUILDING BY THE FSW PROCESS

Luis Carlos Fabrício Filho
luis.fabricio0.lfc@gmail.com; luis.fabricio@ufpe.br

Tiago Leite Rolim
tlr@ufpe.br

Rubens de Andrade Santos
andrade.ruben@gmail.br

Hissae Fujiwara
hissaef84@gmail.com

Ayako Ono
aya.in.brazil@gmail.com

Armando Hideki Shinohara
Federal University of Pernambuco (UFPE), Department of Mechanical Engineering (DEMEC), Recife, Brazil
shinoharaah@yahoo.com; shinohara@ufpe.br

Daniel de Souza Queiroga
Federal University of Pernambuco (UFPE), Center of Informatics (CIn), Recife, Brazil
dsq@cin.ufpe.br

Hidetoshi Fujii
Osaka University, Joining and Welding Reasearch Institute (JWRI), Osaka, Japan
fujii@jwri.osaka-u.ac.jp

Abstract. *The friction stir welding (FSW) process for joining the aluminum alloys is a relatively new and is considered a more interesting method than the traditional arc welding process because the residual stress is substantially low and there is practically no distortion of the welded joint. However, even though from both surfaces of the joint it appears to be free of defects by the visual inspection, internal welding failures such as voids and microstructure changes can be generated during the joining by the FSW process. So, their detection and analysis are fundamental for the improvement of the welding process by the FSW. In the present work, welding of aluminum alloy AA5083 base metal plates for shipbuilding were conducted under supervision of Prof. H. Fujii, authority in FSW, using the facility of Department of Mechanical, Materials and Naval Engineering of UFPE, the aluminum alloy plates and FSW tools provided by JWRI of Osaka University. The detection and characterization of inner defects in the welded joint were conducted by the high spatial resolution digital radiography system using high sensitivity detector Imaging Plate. In order to support to get high quality radiographic images of defects along the welded joint, realistic radiographic numerical simulations were previously conducted with a commercial software.*

Keywords: *aluminum alloy AA5083, shipbuilding, FSW – Friction Stir Welding, defects detection and characterization, digital radiography*

1. INTRODUCTION

The growing concern to mitigate the global warming by reduction of emissions produced by transportation systems that use fossil fuel has led to search for technological and engineering solutions. One of the solutions to this question is

reducing the weight of structures using aluminum alloys, which are low-density lightweight metal alloys with high mechanical strength. According to International Aluminum Institute (2008), "since its first transport applications, aluminum has contributed to reducing the weight of road, rail, marine and aerospace. The demand for aluminum in transport, as well as all other applications, is continuously increasing".

It is well known that the addition of alloy elements to aluminum may enhance mechanical properties. Aluminum alloys of the 5000 series all contain magnesium, ranging from 0.5% up to 12 to13% in weight and the principal benefit adding magnesium and also the silicon is the improvement of the mechanical strength. In shipbuilding, besides the weight reduction for fuel consumption, corrosion resistance is a very important issue. It is well known that aluminum has an excellent corrosion resistance due to the oxide film formation that covers its surface. In special, aluminum alloy AA5083 is suitable for shipbuilding. However, this feature makes welding aluminum to be a challenge. Also, the welding of aluminum presents problems with the solidification from melt, for instance, contraction and porosity generation. Nevertheless, the friction stir welding (FSW) of aluminum and its alloys, developed by The Welding Institute (TWI) in 1991, Cambridge, England, being a solid-state welding process, can solve several of the problems of the traditional arc welding process of aluminum alloys. These characteristics of aluminum alloys and the new welding process have made FSW used for the first time in the marine industry. [Thomas, 2003]. On the other hand, friction stir welded joints are not free from defects. In order to mitigate defects originated during the welding of aluminum alloys, it is fundamental to inspect the friction stir welded joints by using non-destructive tests such as visual, ultrasound and/or radiographic testing for characterization, in order to improve the FSW process, because presence of defects may cause premature failure of the joints.

This work aims to present briefly results of the FSW of AA5083 aluminum alloy using the facilities of Department of Mechanical, Materials and Naval Engineering of UFPE – Federal University of Pernambuco, Recife-PE, Brazil, conducted under supervision of Prof. H. Fujii, authority in FSW, and using aluminum alloys and tools provided by JWRI – Joining and Welding Research Institute of Osaka University, Japan. In special, it aims to present results of inspection of defects detected and characterized in the welded joint by a high sensitivity detector Imaging Plate and high spatial resolution digital radiographic system. Inspection by radiography was conducted in two different directions, 0º and 90º, aiming to detect and determine the size, position and height of the defects. In order to improve the detection limit, Imaging Plate with 100 to 1000 times more sensitive than X-ray film was employed to compensate positioning up 230 cm far from the X-ray source. Furthermore, the digital radiographic images were processed using mathematical filters to enhance the region of interest (ROI). On the other hand, to accelerate obtaining higher spatial resolution radiographs of defects in the welded aluminum alloy joint, radiographic parameters were determined by numerical simulation using a commercial software dedicated to realistic radiography.

2. FUNDAMENTALS OF FSW – FRICTION STIR WELDING AND THE DIGITAL RADIOGRAPHY

2.1 FSW - The Friction Stir Welding

Friction stir welding method is conducted below the melting point of material by pressing a wear-resistant rotating tool that has a pin and a shoulder of larger diameter than of the pin into the joint line. Furthermore, FSW process of joining behaves like a process of constrained extrusion that uses a non-consumable tool, which is traversed along the joint line causing the work pieces to heat, plasticize and be extruded around the part of the tool called pin. Figure 1 shows the schematic of FSW, some types of tools and the welding mechanism principle.

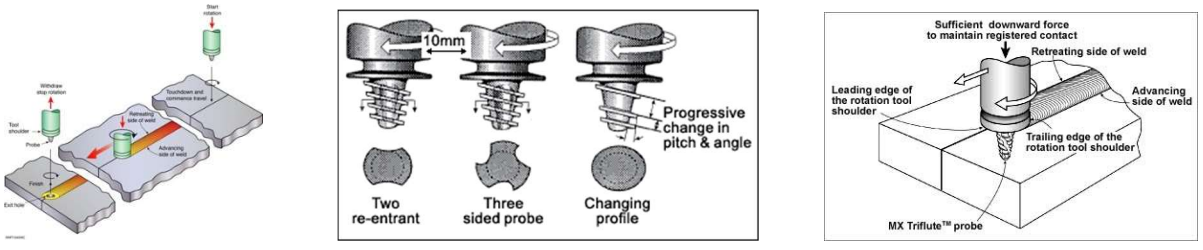

Figure 1. (left) Schematic of the FSW – friction stir welding, (center) types of FSW tools of pin (probe) geometry and (right) welding mechanism principle (Thomas, 2003; DebRoy, 2011).

The material flows around the tool in a very complex way as shown in Fig. 2. It is well known that the material flow depends on the tool geometry, material property and other process parameters, namely rate of rotation and traverse, tool tilt, contact load. Since that are so many parameters involved, defects are likely to occur in joints if the parameters are not well controlled.

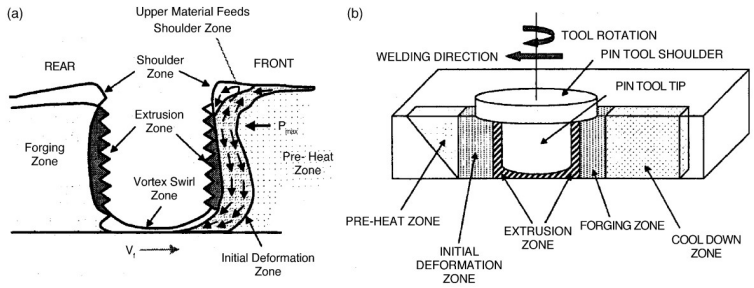

Figure 2. (a) Schematic of the flow of material in FSW – friction stir welding and (b) tool, principle and microstructure [Mishraa, 2005].

2.2 Fundamentals of High Sensitivity and High Spatial Resolution Digital Radiography for Detection of Defects

In radiography, the principle of the use of ionizing radiation for the inspection of structures and internal defects in objects remains unchanged for more than 120 years, since the discovery of the X-rays in 1895 by the German physicist Wilhelm Conrad Röntgen. Object under inspection should be positioned between a source of ionizing radiation and an image detector such as X-ray film, Image Plate (IP) or Digital Detector Array (flat panel). This method of obtaining radiographic images is also known as method of absorption, where a part of the radiation passes through, but another part is absorbed, giving contrast, as shown in Fig. 3(a). Nowadays, it is known that ionizing radiation of X-ray or γ-rays are electromagnetic waves of the same nature of visible light but with wavelength much shorter – of the order of angstrom – which have an interesting property of being able to pass through opaque bodies. As X-ray interacts with electrons of atoms, it has an ability to ionize the atoms of gases, liquids and solid materials, able to pass through materials more easily of materials of lower density. Ability to penetrate materials depends basically on the wavelength of the electromagnetic radiation, "λ", the atomic number "Z" of the material in inspection and the density of the material, "ρ". According to a quantum theory proposed by Planck, the energy of the photons E is given by Eq. 1.

$$E\ (keV) = 12.4\ /\ \lambda\ (\text{Å}) \tag{1}$$

Where "λ" is the wavelength of electromagnetic radiation. In practice, the smaller the wavelength, the higher energy is obtained and consequently the higher the penetration capacity.

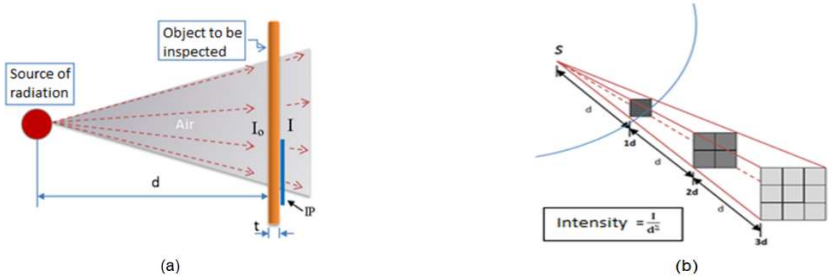

Figure 3. (a) Principle of radiography by method of absorption. The object of interest is positioned between a radiation source and image detector (IP). (b) It shows Newton's law on decreasing the intensity of radiation with the square of the distance.

The relationship between the transmitted (I) and incident (I_0) radiation intensities are given by Eq. (2):

$$I = I_0 e^{-\mu t} \tag{2}$$

Where "t" is the thickness of the object and "μ" is a linear attenuation coefficient that depends on the density "ρ", the atomic number "Z" of the material and the wavelength "λ". Method of absorption is illustrated in Fig. 3 (a).

In addition, when the ionizing radiation is propagated in air, it is known that its intensity per area decreases according to the inverse distance law of Newton, given by Eq. (3); the intensity falls with the square of distance, as is shown in Fig. 3 (b).

$$I_1 \times d_1^2 = I_2 \times d_2^2 \tag{3}$$

In terms of ionizing radiation detectors, there are basically two types of detectors. The so-called pulse meters, such as scintillation counter and proportional counter, which measure photons one by one, are highly sensitive and have a

dead-time of the order of 1 ms. The second type of detector is the so-called integral detector, such as X-ray films and ionization chamber, which provide the total of photons collected during exposure to ionizing radiation. Unlike the pulse and proportional detectors, the integral detectors do not have the dead-time problem, but generate relatively more noise, thus reducing the S / N (signal / noise) ratio of the detector.

In the 1980s, for a medical application, Fuji Film of Japan developed an innovative two-dimensional detector for radiography, called Imaging Plate (IP), using the crystal luminescence phenomenon (BaFBr: Eu^{2+}). The IP detector brings together features of integral and pulse detectors. In 1985, the IP characteristics were investigated and tested with success for the X-ray detector in diffraction techniques for the study of crystalline structures of biological materials – which present naturally low diffraction intensity, X-ray scattering with synchrotron radiation. The study revealed the following characteristics: very high sensitivity, reaching up to three orders of order higher compared to a conventional X-ray film; extremely dynamic range; linearity; excellent spatial resolution of the order of 25 μm. To obtain the image from the IP, a laser scanner (scanner) scans the digital data to the computer for further processing of images. There is no need to use darkroom and neither chemicals such as fixer and developer, as required by conventional X-ray film. Figure 4(a) shows the exceptional sensitivity and linearity of IP over conventional X-ray film when both were submitted to different doses of ionizing radiation. The abscissa corresponds to radiation doses emitted by a standard sample of ^{32}P (beta radiation of energy : $E = 1{,}7$ MeV).

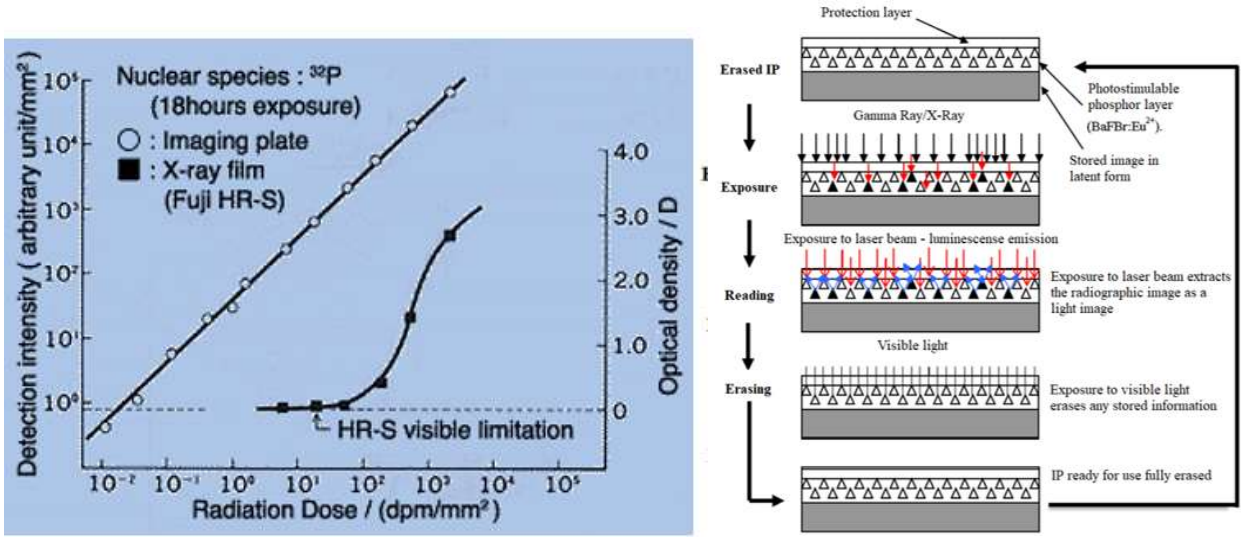

Figure 4. (Left) The exceptional sensitivity of the IP is compared to the one of the X-ray film. (Right) Procedure of processing of IP: exposure, reading, erasing and reuse (Shinohara, 2017).

In Fig. 4 (left), the ordinate axis at the left represents the amount of luminescent radiation accumulated by the IP and the right one shows the optical density, degree of darkness of an X-ray film. These characteristics are also similar for radiation of electron beams, X-rays, γ-rays and beta particles of different energies. These features of the IP detector open new applications not yet explored. Fig. 4 (right) presents a simplified scheme of the operation and processing usually adopted in practice to carry out radiography with the IP detector. Detailed procedure can be found, for example, in the ASTM E2007-10 standard (reapproved in 2016). After the exposure of IP to radiation, the radiographic image is stored in latent mode in the crystals of (BaFBr: Eu^{2+}), but soon after exposure to ionizing radiation, a process of loss of information begins due to the effect known as fading. The process called OSL - Optical Stimulated Luminescence, which is a nonlinear effect, is used to perform the retrieval of the information of radiographic image stored in the IP. For example, when the 632 nm He-Ne laser beam impinges the IP surface, 488 nm luminescence emission occurs by effect of the OSL. A photomultiplier tube (PMT) captures the luminescence emission and then an analogical to digital converter (ADC) converts to digital signal and the image is shown in the computer monitor. Further processing can be done by dedicated image processing software. To reuse the IP, it is exposed for a few minutes in an eraser using white light. For industrial application, depending on the IP handling, it can be reused up to 1,000 times.

In radiography, the formation of images occurs due to the contrast of the direct beam of radiation when it passes through the object and also by the scattered radiation resulting from the interaction of the radiation with the matter, which reduces the contrast. Fig. 5 (a) schematically illustrates the effect of scattered radiation on the passage of radiation by the object of interest in a numerical simulation. Numerical simulations of radiographic images can take into account scattered photons using Monte Carlo computation, which is responsible for a more accurate computation. The scattered radiation carries no information about the internal structure.

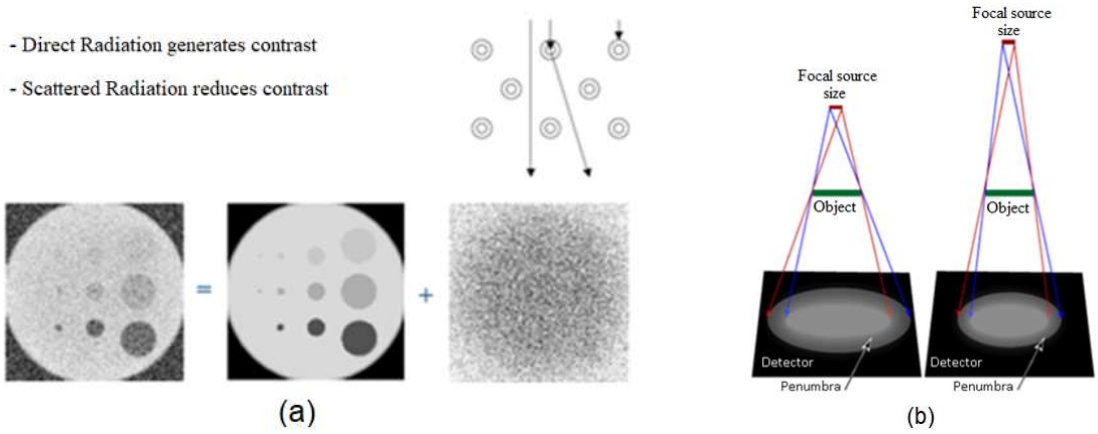

Figure 5. (a) Effect of scattered radiation by matter on contrast reduction (CIVA-RT). (b) Scheme of reduction of geometrical unsharpness changing the distance of radiation source from the object under inspection.

In practice, there are four factors that most affect image quality in industrial radiography: (1) Geometrical unsharpness, U_g, due to the size of the source of the radiation (focal spot); (2) Unsharpness of the film, U_f, due to the scattering of the electrons in the detector; (3) Unsharpness due to image intensifier, U_s, caused by scattering of light in the fluorescent layer; (4) Unsharpness due to motion, U_{mv}, due to the relative movement of the object and film. The last two are less critical when radiography is conducted in the laboratory. In order to reduce the effect of the geometrical unsharpness, U_g, an interesting practice is to position the radiation source as far as possible from the object of interest, as shown in the schematic Fig. 5 (b). In this case, the intensity of radiation decreases as a function of the square of the distance, according to Newton's Law. As a consequence, in order compensate longer exposure time, the use of high sensitivity detector such as Image Plate is interesting. In terms of the spatial resolution of the IP, which is related to the unsharpness of the detector, U_f, it refers to the ability to discern details. Currently, there are two types of commercially available IP, which are "standard" (highest sensitivity but relatively lower spatial resolution) and "blue" type which shows high sensitivity than traditional X-ray film, but lower than the "standard" IP; however, it has a higher spatial resolution among the IP.

3. MATERIALS AND METHODOLOGY

3.1 Base Material Aluminum Alloy AA5083 for Shipbuilding and FSW Process

The aluminum alloy for welding using the FSW process consists of base material AA5083 plates of 300 mm long, 50 mm wide and 5 mm in thickness provided by JWRI/Osaka University, from Japan.

The FSW joining process of the aluminum alloy was conducted in November of 2016 aiming to introduce the technique for the first time in Pernambuco State, under supervision of Prof. H. Fujii, who is authority in FSW and delivered an intensive course on FSW as Project Based Learning (PBL) mode at Campus of UFPE in Recife for students and faculty members of mechanical, materials and naval engineering of UFPE, because the most modern and advanced shipyard of the South America is installed in this State and 2011, UFPE established undergraduate course in Naval Engineering. The aluminum alloy AA5083 plates were joined using universal milling machines with electrical motor of 7.5 HP of Department of Mechanical Engineering of UFPE. The used tool has a columnar shape with a screw probe made of SKD61 steel. The diameter of the shoulder was 15 mm. The diameter and the length of the probe were 5 and 4.9 mm, respectively, and the tilt angle of probe was 3°. A shipbuilding steel plate of 19 mm in thickness was used for the backing plate.

For present work, two specimens were prepared for radiographic inspection. For preparation of the specimen named AA5083_01, the tool rotation speed was set to be 800 rpm and the welding speed was 106 mm/min. The specimen named AA5083_02, the tool rotation speed was also 800 rpm but the welding speed was 210 mm/min. For both welding, the tool rotation was in the clockwise direction. The rotation rate and welding speed were chosen from previously determined condition for aluminum alloy AA5083, as show in Fig. 6. To start the FSW joining of base metals, the penetration depth of the tilted tool into the base metals was conducted visually determining the downforce, in order to control the welding process aiming to get a sound joint. The fixation of base metals is one fundamental parameter to get good result. It was made as better possible because the downforce and welding speed have considerable influence on results.

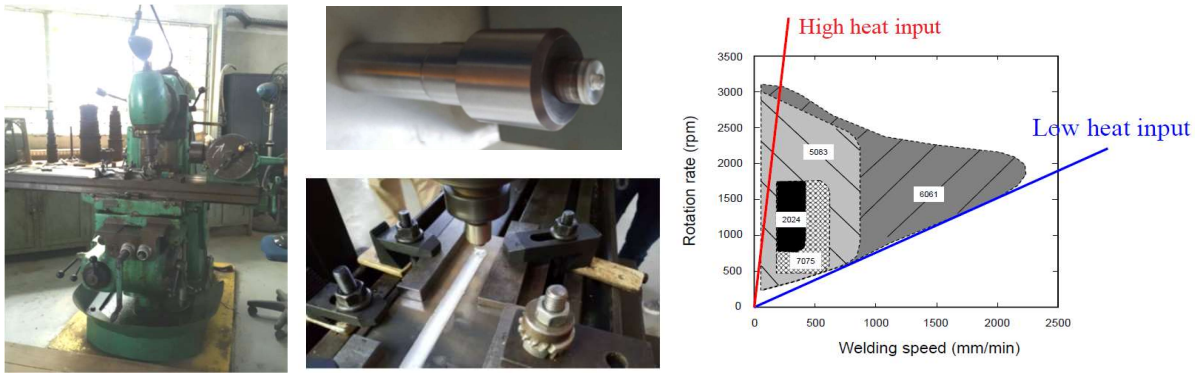

Figure 6. (left) Photo of milling machine, (center) tool employed for welding and fixation system and at (right) chart of FSW process of aluminum alloys taking into consideration the heat input as a function of rotation rate and welding speed.

3.2 Numerical Simulation of Radiography

In principle, aluminum and its alloys is an interesting material to be inspected by radiography technique in comparison to steel materials because it is lightweight material, lower density. So, it is relatively easier to X-ray radiation pass through of aluminum alloy and to detection of inner defects results in higher contrast. In order to determine basic radiographic parameters, a study was conducted before experimental testing to avoid exposure to ionizing radiation and to speed up to get high quality radiographic imaging of defects. In the present study, a commercial CIVA-RT, version 11.0 software for numerical simulation for realistic radiographic was used. First, a numerical simulation investigation was conducted aiming to define the parameters reproducing a real radiographic image of aluminum alloy AA5083_01 joint and its defects. After that, several radiographic parameters were tested taking into consideration the scattering of X-ray in the matter using Monte-Carlo to simulate the scattering using 60 kV, 90 kV and 120 kV and varying the distance of X-source to the specimen up 230 cm. The numerical simulation was conducted in two directions, one of direction is perpendicular to the joined plate and other direction is parallel to the plate.

3.3 Digital Radiography System and Image Processing

The X-ray source used for detection and characterization of defects in the welded joint was a battery powered ICM CP-120B model, made in Belgium. The maximum power of the X-ray source was 120 kV and 1 mA. The focus size is 0.5 mm x 0.8 mm. In the present work, the distance of X-ray source from the joined alloy was up to 230 cm. The acceleration voltages tested were: 60 kV, 90 kV and 120 kV. The laser scanner to read the IP was the highest resolution available in the market model HD-CR 35 NDT, Durr, Germany and certificated by BAM – Federal Institute of Materials and Testing, Berlin, Germany. For recording radiographic image, IP of Dürr® , blue type of two different sizes were employed: (i) 240 mm long and 100 mm wide and (ii) 240 mm long and 180 mm wide IPs. In order to determine which voltage was more interesting for contrast, an aluminum step-wedge shown in Fig. 7 (a) was used. Figure 7 (b) shows schematic figures the two directions radiographic testing of welded joint. The as-obtained radiographic images were analyzed and processed with Isee! software, from BAM.

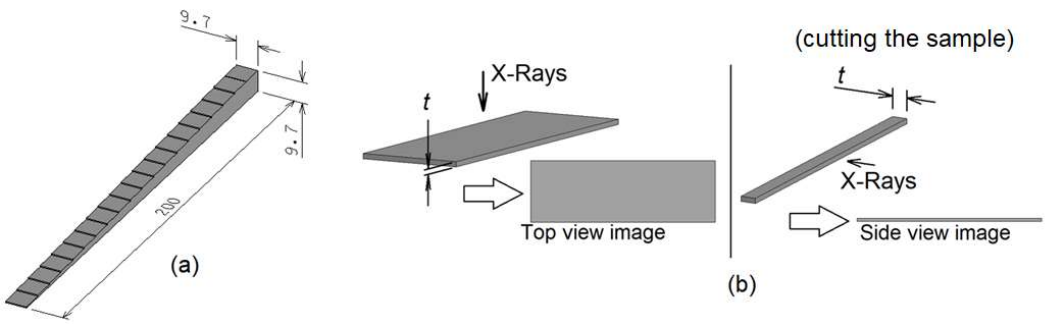

Figure 7. (a) Aluminum step wedge with its dimension. The step was 0.5 mm. (b) Schematic figures for top and lateral radiography.

4. RESULTS AND DISCUSSION

For the present work, two sets of specimens of aluminum alloy AA5083 were prepared by the FSW process at Department of Mechanical of Mechanical, Materials and Naval Engineering of UFPE and results are shown in Fig. 8 and 9. No lack of bonding was observed on both specimens by visual inspection.

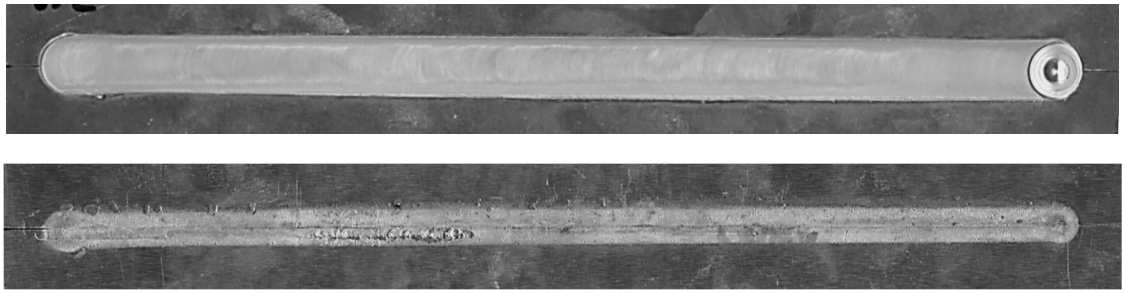

Figure 8. High resolution photos of welded joint by FSW of specimen AA5083_01, showing top side with end of welding and at bottom, back side. Both sides seem to be free of defects such as lack of bonding.

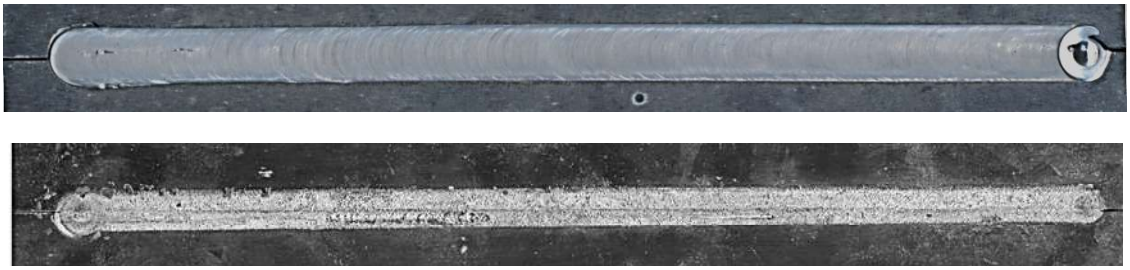

Figure 9. High resolution photos of welded joint by the FSW of specimen AA5083_02, showing top side with end of welding with a hole and at bottom, the back side. No big apparent defects are present on both sides.

The results of numerical simulation of radiography of aluminum alloy of AA5083 plates are shown in Fig. 10 for two different distances (from X-ray source to specimen): 60 cm and 250 cm using 120 kV of acceleration voltage. As a result, in both cases, the simulated inner defects are detected in simulated radiography. In principle, the farthest the X-ray source is from the specimen, the better is the definition of the defect on the radiography. But, from the numerically simulated radiographies, that difference was not clearly visible.

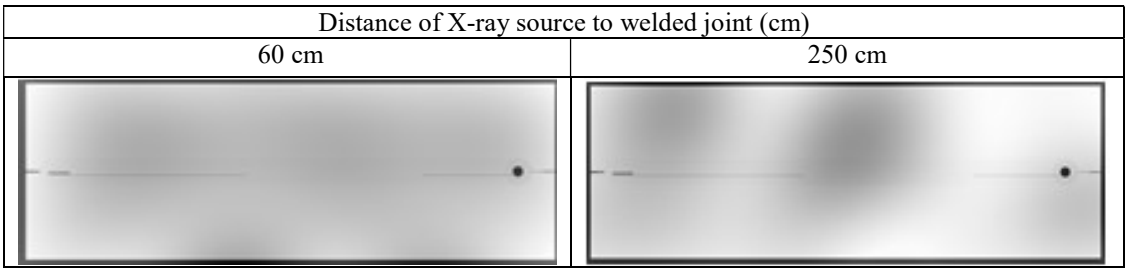

Figure 10. Numerical simulation of welded joint of AA5083 plate with 5 mm in thickness. The exposure time: 30 s; Voltage: 120 kV; Current: 1 mA

Furthermore, the lower voltage is used, the value of linear absorption coefficient "μ" becomes higher. As a consequence, the contrast of defects should be better according to Eq. 2. In order to verify this hypothesis, three voltages were tested: 60 kV, 90 kV and 120 kV using an aluminum step wedge (Fig. 7(a), schematic). The results of radiographs are shown in Fig. 11 and contrast is better when using 60 kV. The higher the voltage, the higher the energy and the lower the wavelength λ. Since the linear attenuation coefficient μ depends on the wavelength λ, μ decreases as the voltage increases. From Eq. 2, it is shown that a decrease of μ causes the I / I_0 ratio to tend to 1 exponentially. Therefore, as expected, the contrast decreases for higher voltages.

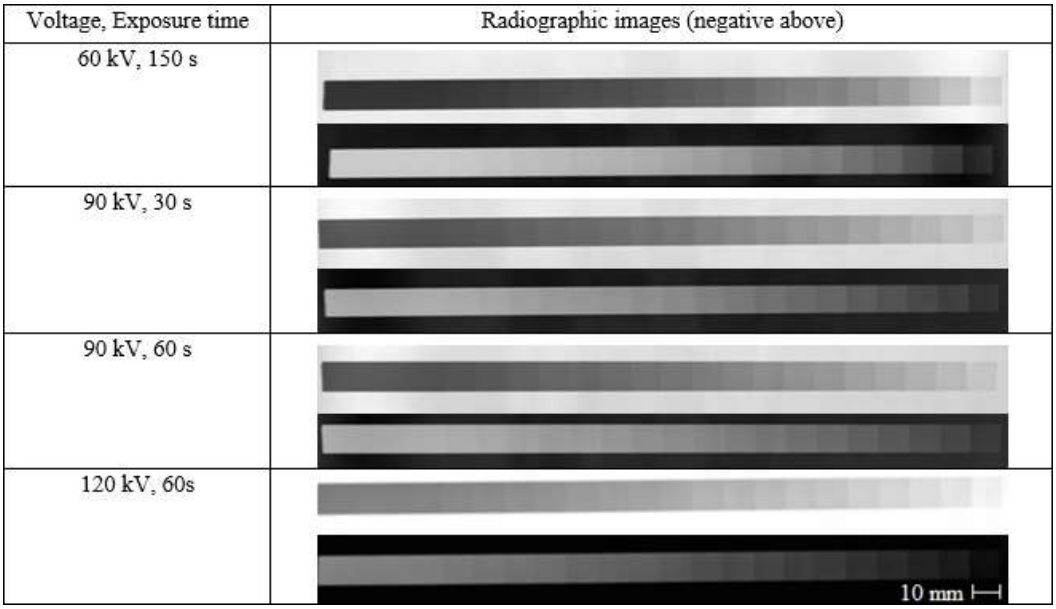

Figure 11. shows the contrast results of step-wedge radiography with different acceleration voltage.

Radiographic inspection of specimens AA5083_01 with 60 kV and 120 kV are shown in Fig. 12. For the specimen, it is clear from images that radiography taken with 60 kV gives more contrast than radiography taken with 120 kV. From the both radiographs, beyond of clear detection of two lines of flash, is possible to see a narrow line-like defect from start to end of FSW welding and the line defect is slight dislocated from the joint line. Those observations are more clearly shown in Fig. 13 with application of pseudo plastic filter, of Isee! software Pseudo plastic" filter, of Isee! Software.

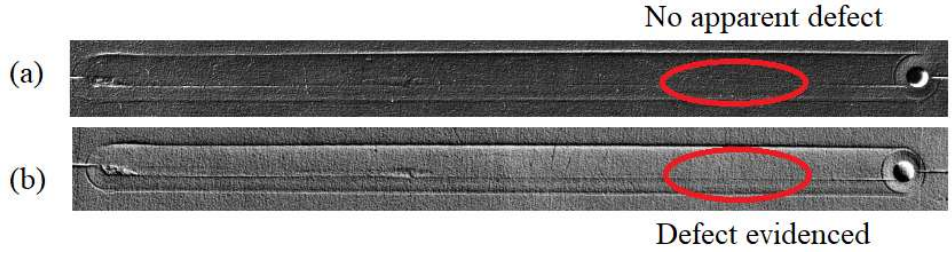

Figure 12. Comparison between the contrast generated in the sample AA5083_01 by (a) 120 kV and (b) 60 kV

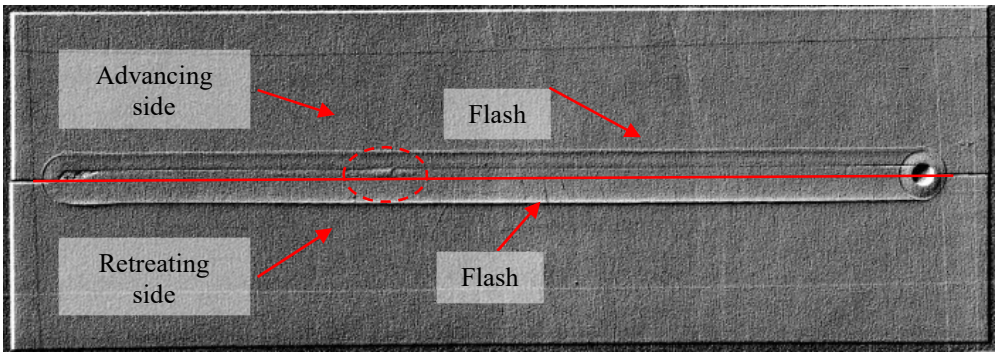

Figure 13. Identification in radiographic detection of defects in AA5083_01 specimen.

So, from this section, results of radiography taken with X-ray radiation with 60 kV will be presented because radiation could pass through of the AA5083 plate and showed better contrast than higher voltages. The analysis of a supposed defect detected in Fig. 13 – circled with dashed red line – with the help of visual inspection of the back side of the welded joint (see Fig. 14), makes us understand that that is nothing but an excessive deposition of welded aluminum on the back side of welded joint.

Figure 14. High resolution photo taken of back side of welded joint showing excessive deposition of aluminum during welding by FSW process.

Figure 15 shows radiographic images of two specimens welded using the same rotation rate but different speed of welding. In the both specimens, narrow line-like defect appears dislocated from joint line but the higher welding speed, the worse the inner defects become. The origin of narrow line-like defect along the welding can be attributed to complex material flow during welding generating a cavity. Material moves from the advancing side to the retreating side. As can be seen on the radiographic image, the defects occur on the advancing side. On the other hand, in the retreating side, there is a mass of material (denominated flash) which was ejected during the FSW process due to the heat input, because it leads to the softening of the material. The heat input was higher in sample AA5083_01 than in sample AA5083_02.

Sample name	Welding parameters	Post-processed radiographic images
AA5083_01	800 rpm, 106 mm/min	
AA5083_02	800 rpm, 210 mm/min	

Figure 15. Post-processed radiographic images of the samples.

So, the high spatial resolution radiographic system used could detect several kinds of defects in one direction. In order to detect at 90º, welded joint region of interest of the specimen AA5083_01 was cut out as shown in Fig. 16.

Figure 16. A photo of specimen cut out from AA5083_01 and its size is 300 mm long, 12.5 mm wide, 5 mm thick.

Figures 17 show the obtained radiographic image of the cut AA5083 specimen (positive and negative colors) and the same image after processing with pseudo-plast filter, featuring regions close to start of the welded joint. The importance of the post-processing is perceived from this figure. Figure 18, in turn, shows the post-processed image featuring regions close to start of the welded joint of the same sample. Radiographic parameters were: 60 kV, 1 mA, exposure time of 120 s and X-ray source distance from de specimen 60 cm.

Radiographic images of the cut out specimen of AA5083_01	
Original image	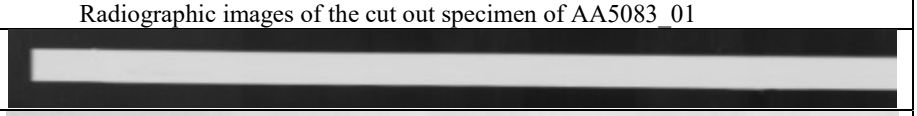
Negative image	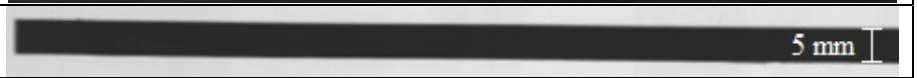
Post-processed image	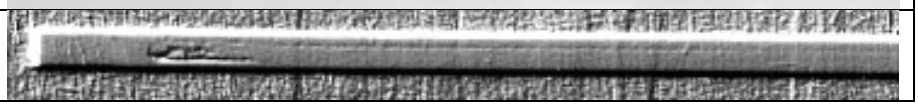

Figure 17. Radiographic images of the cut out specimen from AA5083_01. Post-processed image with pseudo-plast filter (X shift = 21, Y shift = 21, GV offset = 300) and with grey scale adjustment.

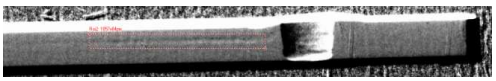

Figure 19. Narrow line-like defects can be seen on side radiography of cut out specimen AA5083_01 close to the end of the welded joint.

From those radiographs, it is possible to see better that the narrow line-like defect appears closer to upper surface (top side), and the defect at start point in the bottom part of plate. Figure 19 show the final part of welded joint.

The line-like defect keeps the same height since the start. IP blue type of 100 mm x 240 mm was used. IP read by laser was conducted with highest resolution of 20 μm.

5. CONCLUSIONS

Plates of Aluminum alloy AA5083 for shipbuilding were successfully joined for the first time in Pernambuco.

Using digital radiography system facility of Department of Mechanical, Materials and Naval Engineering of UFPE, several kinds of inner defects could be detected and characterized. Furthermore, the use of a lower voltage of X-ray source, digital image processing, better contrast and information about defects can be obtained. Information about defects is particularly useful to support the improvement of the FSW of aluminum alloys.

As a future work, in addition to developing a better fixation system for the aluminum plates to carry out the welding, investigating the inner defects through CT – computed tomography of high resolution – is recommended for better understanding the defects generated and the FSW of aluminum alloy.

6. ACKNOWLEDGEMENTS

The authors acknowledge the support of Joining and Welding Research Institute (JWRI) of Osaka University, Japan, for providing aluminum alloys and FSW tools to conduct PBL - Project Based Learning intensive course at UFPE in Recife, coordinated by Prof. Hidetoshi Fujii, and his assistants Mr.Takuya Wada and Mr. Yo Aoki.

7. REFERENCES

Dawes, C. J. and Thomas, W. M. 1996. “Friction stir process welds aluminum alloys”, Weld. J., 75, (3), 41–45.

Fernandes, C. A., Urtiga Filho, S. L., Shinohara, A. H. and Fujii, H., 2017. “Avaliação mecânica e microestrutural de juntas soldadas por fricção e mistura mecânica da liga de alumínio 6061”. May 2017. *Coteq 2017: 14ª Conferência sobre Tecnologia de Equipamentos.*

Haboudou, A., Peyre, P., Vannes, A.B. and Peix, G. 2003. “Reduction of porosity content generated during Nd:YAG laser welding of A356 and AA5083 aluminium alloys”. *Materials Science and Engineering*: *A*, Vol. 363, Issues 1–2, p. 40-52

International Aluminium Institute, 2008. “Transport and Aluminium”. 15 Jan 2013 <http://www.world-aluminium.org/media/filer_public/2013/01/15/fl0000172.pdf>

ISEE! Bundesanstalt Für Materialforschung Und Prüfung. < http://www.dir.bam.de >

Johnson, R. and Threadgill, P. L., 2003. “Progress in friction stir welding of aluminium and steel for marine applications”. Oct 2003. *RINA Conference: Advanced Marine Materials: Technology and Applications*.

Kim, Y.G., Fujii, H., Tsumura, T., Komazaki, T. and Nakata, K., 2006. “Three defect types in friction stir welding of aluminum die casting alloy”. *Materials Science and Engineering: A*, Vol. 415, p. 250-254.

Mishraa, R.S., Mab, Z.Y. 2005. “Friction stir welding and processing”. *Materials Science and Engineering* R 50, p. 1–78

Nicholas, E. D. and Thomas, W. M. 1998. “A review of friction processes for aerospace applications”, *Int. J. Mater. Prod. Technol*., 13, (1–2), p. 45–55.

Peel, M., Steuwer, A., Preuss and M., Withers, P.J. 2003. “Microstructure, mechanical properties and residual stresses as a function of welding speed in aluminium AA5083 friction stir welds”. *In Acta Materialia*, Vol. 51 (16), p. 4791-4801.

Rai1, R., De, A., Bhadeshia, H. K. D. H. and DebRoy, T. 2011. “Review: friction stir welding tools”. *Science and Technology of Welding and Joining*. Vol. 16(4) p. 325.

Shinohara, A. H., Silva Jr, E. J., Xavier, G. J. V., Fujiwara, H., Nonaka, J., Lott Neto, H. B. D. T., Britto, P. R. R., and Fontan, M. A. B., 2017. “Sistema Radiográfico Digital para Detecção de Falhas Mecânicas Ocultas nos Isoladores Poliméricos em Linhas de Transmissão de 500 kV Energizadas”. In *Proceedings of the 17th Iberoamerican Regional Meeting of the Cigré – XVII ERIAC*. Ciudad Del Este, Paraguay.

Thomas, W. M. 2003. “Friction stir welding – recent developments”, *Mater. Sci. Forum*, p. 426–432.

Thomas, W. M., Nicholas, E. D., Needham, J. C., Murch, M. G., Templesmith, P. and Dawes, C. J. 1995. “Friction stir butt welding”, US Patent 5460317.

8. RESPONSIBILITY NOTE

The authors are the only responsible for the printed material included in this paper.